Role of ammonia on fine-particle pH in agricultural regions of China: Comparison between urban and rural sites

Shenbo Wang [a], Lingling Wang [b], Yuqing Li [c], Chen Wang [a], Weisi Wang [b], Shasha Yin [a, *], Ruiqin Zhang [a, *]

[a] *Research Institute of Environmental Science, College of Chemistry, Zhengzhou University, Zhengzhou, 450001, China*

[b] *Department of Environmental Protection of Henan Province, Zhengzhou, 450001, China*

[c] *Department of Environment Science and Engineering, Tsinghua University, Beijing 100084, China*

* Corresponding authors：Shasha Yin and Ruiqin Zhang

E-mail addresses: shashayin@zzu.edu.cn；rqzhang@zzu.edu.cn

Abstract: Particle acidity is a fundamental property that affects atmospheric particulate chemistry. Synchronous online monitoring was performed in two urban sites (e.g., Zhengzhou (U-ZZ) and Anyang (U-AY)) and three rural sites (e.g., Anyang (R-AY), Xinxiang (R-XX), and Puyang (R-PY)) in Henan Province during a haze episode to investigate the pH value and its driving factors in the agricultural regions of China. The pH values of particles calculated by ISORROPIA-II model at rural sites were slightly higher than those at urban sites, with the median (min–max) values of 5.2 (4.8–6.9, R-PY), 5.1 (4.7–6.5, R-AY), 4.9 (4.1–6.8, R-XX), 4.8 (3.9–5.9, U-AY), and 4.5 (3.8–5.2, U-ZZ). Sensitivity tests show that TNH_x (total ammonium (gas + aerosol)), followed by total sulfate, were the important factors that influenced the predicted pH. Generally, particle pH increased with the cation increasing and the decrease in the anion, temperature, and relative humidity. Similar pH values (~3.0) at the required NH_x concentrations for the five sites indicated that the presence of excess NH_x was likely important for the less acidic of $PM_{2.5}$ during the severe haze episodes in this region. Moreover, the concentrations of excess NH_x may drive the higher pH values at rural sites, because of the higher excess NH_x concentrations at rural sites than those at urban sites. The underlying influence of regional transport on local particle pH cannot be neglected by differing the chemical components of $PM_{2.5}$ and meteorological conditions. Air masses transported from rural and agricultural regions may enhance the particle pH value in urban aerosols given the high pH of particles and high ammonia levels. These results suggest that ammonia is urgently needed to be involved in the regional strategy for the improvement of air quality in China.

Keywords: ISORROPIA-II model, Particle acidity, Ammonia, Sensitivity test, Regional transport.

1 Introduction

High concentrations of acids and bases contained in the aqueous phase define the acidity of aerosols (Spurny, 1990). Particle acidity or pH value is an important parameter for atmospheric particulate chemistry, such as the gas-particle portioning of semi-volatile and volatile species (e.g., $NH_{3(g)}/NH_{4(aq)}^{+}$, $HCl_{(g)}/Cl_{(aq)}^{-}$, and $HNO_{3(g)}/NO_{3(aq)}^{-}$), the formation of secondary inorganic and organic aerosols, and the dissolution of metallic elements (Bougiatioti et al., 2016; Meskhidze et al., 2003; Seinfeld and Pandis, 2006; Shi et al., 2019; Shi et al., 2010; Surratt et al., 2010; Wang et al., 2018b). Particle acidity can affect the ecosystem through its influence on wet/dry deposition, atmospheric visibility, and radiative balance (Boucher and Anderson, 1995; Larssen et al., 2006; Pye et al., 2019; Watson, 2002). In addition, high particle acidity has an adverse impact on public health, especially for the cardiopulmonary and respiration system of humans (Dockery et al., 1996; Ostro et al., 1991).

Direct measurements on particle pH are challenging because of the small size and nonideality of chemical species in solvated aerosols. Therefore, thermodynamic models, such as E-AIM (http://www.aim.env.uea.ac.uk/aim/aim.php) and ISORROPIA-II (http://isorropia.eas.gatech.edu) (Clegg et al., 1998; Nenes et al., 1998), which rely on the measurements of particulate and gaseous species, are widely used in estimating particle pH. Generally, the global distribution of fine particulate matter ($PM_{2.5}$, aerodynamic diameter $\leq$ 2.5 μm) pH is bimodal with a population of particles having a mean pH of 1–3 and another population having an average pH closer to 4–5 (Pye et al., 2019). Table 1 shows that $PM_{2.5}$ in mainland China were moderately acidic with pH values that ranged from 3.4–5.7 (Ding et al., 2019; Guo et al., 2017; Liu et al., 2017; Shi et al., 2017, 2019; Song et al., 2018; Wang et al., 2019a), which were 3–5 units higher than those reported in other regions, such as Hong Kong,

Singapore, USA, and Greece (Behera et al., 2013; Bougiatioti et al., 2016; Guo et al., 2016; Guo et al., 2014; Pathak et al., 2004).

High atmospheric ammonia (TNH_x, gas NH_3 plus particle NH_4^+) is a dominant factor that drives the high $PM_{2.5}$ pH in megacities of China because it suppresses the production of particle hydronium (Cheng et al., 2016; Wang et al., 2016). Liu et al. (2017) argued that excess NH_3 and elevated aerosol water content (AWC) were responsible for the high pH in Beijing. Nevertheless, Guo et al. (2017) and Song et al. (2018) demonstrated that high levels of ammonia did not increase the $PM_{2.5}$ pH into a fully neutralized condition in Beijing and Xi'an, China. Weber et al. (2016) calculated that only large increases in NH_3 together with sulfate reductions can lead to an increase in pH. Correspondingly, higher pH by about 1 unit than urban aerosols was observed in locations of intensive agriculture with high NH_3 concentrations in the southeastern US (Nah et al., 2018). The primary sources for ammonia include agricultural emissions, such as livestock waste, N-fertilizer application, and biomass burning, as well as traffic and industrial emissions (Huang et al., 2012; Shen et al., 2011; Wang et al., 2018a). Field studies have reported that elevated NH_3 and NH_4^+ concentrations were recorded at rural sites in the North China Plain (Meng et al., 2011; Meng et al., 2017; Shen et al., 2011; Wen et al., 2015). Therefore, studying in an agriculturally developed region is needed to obtain insight into the role of ammonia in particle pH. Unfortunately, previous studies mainly concentrated on calculating the particle pH in the megacity of China, and few studies focused on the agricultural regions of China. In addition to ammonia, particle pH can also be influenced by other chemical compositions and meteorological conditions, such as sulfate, AWC, temperature (T), and relative humidity (RH). Sulfate is often the main acid component of aerosols, and largely determines the acidity of $PM_{2.5}$ (Weber et al.,

2016). Sensitivity tests in Beijing suggested that sulfate, TNH_x, and T were the common driving factors, and Ca^{2+} and RH were the unique factors in special seasons (Ding et al., 2019). The pH sensitivity based on the 10-year record in Canada showed that chemical compositions had various effects on particle pH under different meteorological conditions; moreover, careful examination for any particular region is needed (Tao and Murphy, 2019).

Henan Province is situated in Central China; it has a dense rural population and is a top-ranking province in China in terms of agricultural production and chemical fertilizer consumption (NBS, 2016). NH_3 emission inventory for Henan Province reported that approximately 1031.6 Gg NH_3 was released in Henan in 2015, thereby contributing to approximately 10 % of China's total emissions (approximately 10 Tg) (Huang et al., 2012; Wang et al., 2018a). Livestock waste and N-fertilizer application were major sources for ammonia emissions, which may increase TNH_x concentrations at rural sites than in urban sites. Furthermore, Henan Province is a severely $PM_{2.5}$-polluted region in China. In January 2018, a large-scale and long-lasting haze episode that caused $PM_{2.5}$ concentration to reach 400 $\mu g/m^3$ occurred in this region (Wang et al., 2019c). An experiment was performed in two urban and three rural sites in Henan Province to investigate the particle acidity and its driving factor. ISORROPIA-II model was utilized to estimate $PM_{2.5}$ pH using a high-time-resolution dataset. The novelty of the work addressed in the present study is that this study is the first on $PM_{2.5}$ acidity by comparing urban and rural sites in the agricultural regions of China. The specific objectives of the study were presented as follows: (1) Estimation and comparison of the $PM_{2.5}$ pH at the five monitoring sites, (2) identification of the factors that determine the pH, and (3) discussion of the role of ammonia on pH. Our results are helpful to understand the factors that determine particle acidity better.

2 Experiment and methods

2.1 Site descriptions

Field sampling was synchronously conducted from January 12 to 24, 2018 at five sites (i.e., two urban sites located in the center of Zhengzhou (U-ZZ) and Anyang (U-AY), and three sites located in the rural areas of Anyang (R-AY), Xinxiang (R-XX), and Puyang (R-PY)). Locations of the five sites (Fig. S1) with brief descriptions are listed in Table 2. U-ZZ site is surrounded by busy roads, and two freeways are located 3 km to the south and 7 km to the east. Moreover, this site is near a coal-fired power plant; a gas-fired power plant; and several small-scale industries, such as pharmaceutical companies, electronic factories, and equipment manufacturing. U-AY site is surrounded by busy roads, and Anyang steelwork is located 8 km to the west. R-AY site is surrounded by farmland and is 1 km west of the Jing-Gang-Ao freeway and 1 km north of a belt freeway. R-XX and R-PY sites are surrounded by farmland without other prominent anthropogenic emission sources.

2.2 Instrumentations

The hourly mass concentrations of water-soluble inorganic ions (WSIIs) in $PM_{2.5}$, such as NH_4^+, SO_4^{2-}, NO_3^-, Cl^-, Na^+, Mg^{2+}, Ca^{2+}, and K^+ and their gaseous precursors (i.e., NH_3, HNO_3, and HCl) were measured using an ambient ion monitor (URG-9000D, Thermal Fisher Scientific, USA) in U-ZZ site and the monitor for aerosols and gases (MARGA, Metrohm, Switzerland) in other sites. Both instruments have been successfully deployed in several other field experiments (Li et al., 2017; Shi et al., 2017; Wang 2019b), and detailed information is available elsewhere (Markovic et al., 2012; Rumsey et al., 2014). As a brief summary, ambient air is drawn into the systems at a flow rate of 16.7 L/min. Subsequently, particles and gases are collected by two aerosol sample collectors through a wet

126 parallel plate or wet rotating denuder. Aqueous solution samples are quantified by using two ion
127 chromatography analyzers. Detection limits for all species during the sampling periods were less than
128 0.1 μg/m^3. Measurement uncertainties were assumed to 10 % for URG-9000D here by reference to
129 10 % of Markovic et al. (2012) and 12 % in Hu et al. (2014). For the MARGA instrument, Song et al.
130 (2018) took 20 % as overall relative uncertainties for major species, and Rumsey et al. (2014) reported
131 that the analytical biases were lower than 10 % for SO_4^{2-}, NO_3^-, and HNO_3, but higher than 15 % for
132 NH_3 and NH_4^+. Therefore, overall uncertainties were estimated to be 20 % for NH_3 and NH_4^+ and 10 %
133 for other species. The combined uncertainties for TNH_x were calculated to be 14 % and 23 % for U-
134 ZZ and other sites, respectively, and 14 % uncertainties of TNO_3 ($NO_{3(aq)}^-$ + $HNO_{3(g)}$) and TCl ($Cl_{(aq)}^-$
135 + $HCl_{(g)}$) for all sites. Because of the complex interference during sampling periods at the five sites,
136 such as the slope from the internal calibration, the solution volume, temperature, pressure, and airflow
137 rate, the actual uncertainties might be different from the estimated value. Hourly elemental carbon (EC)
138 and organic carbon (OC) concentrations in $PM_{2.5}$ were simultaneously obtained by the semi-
139 continuous carbon analyzers (Model 4, Sunset Laboratory Inc, USA) in the same place, except for the
140 U-ZZ site, of which data were provided by the Department of Environmental Protection of Henan
141 Province. Detailed information on this instrument can be found in Panteliadis et al. (2014). Briefly,
142 $PM_{2.5}$ collected by the device was oxidized to carbon dioxide and analyzed by a nondispersive infrared
143 detector. The relative measurement uncertainty for this instrument was estimated to be 20 % (Liu et
144 al., 2013; Healy et al., 2013). Meteorological parameters, including T, RH, wind direction, and wind
145 speed, were recorded by smart weather sensor (LUFFT-WS500, Sutron Corporation, Germany), with
146 the accuracies of ± 0.2 ℃, ± 2 %, < 3 °, and 0.1 m/s, respectively.

2.3 pH prediction

Particle pH was estimated using the ISORROPIA-II thermodynamic model. Input data, including RH, T, concentrations of K^+, Ca^{2+}, Mg^{2+}, TNH_x, total sulfate (TH_2SO_4, replaced by observed SO_4^{2-}), total sodium (TNa, replaced by observed Na^+), TCl, and TNO_3, were used to calculate the particle hydronium ion concentration per volume of air (H^+_{air}) and particle water associated with inorganics (AWC_{inorg}) by computing the equilibrium composition for the Na^+-K^+-Ca^{2+}-Mg^{2+}-NH_4^+-SO_4^{2-}-NO_3^--Cl^--H_2O aerosol system. Considering that forward mode is less sensitive to measurement error than the reverse mode and high RH levels were recorded in sampling periods, ISORROPIA-II was run in the forward model for the aerosol system in the metastable condition (Ding et al, 2019; Guo et al., 2015; Hennigan et al., 2015). Moreover, we excluded data with RH < 30 %, a condition where predicted to observed partitioning of nitrate between the gas and particle phase are in weak correlation, and thus uncertainties in the pH prediction are expected to be high (Ding et al., 2019; Guo et al., 2016). Aerosol pH was calculated according to the formula (Bougiatioti et al., 2016):

$$\mathrm{pH} = -\log_{10} H^+_{aq} = -\log_{10} \frac{1000 H^+_{air}}{AWC_{inorg} + AWC_{org}}, \quad (1)$$

where the modeled concentrations for AWC_{inorg} and H^+_{air} are μg/m^3, and AWC_{org} is the particle water associated with the organics predicted using the method:

$$AWC_{org} = \frac{m_s}{\rho_s} \frac{k_{org}}{\left(\frac{1}{\mathrm{RH}} - 1\right)}, \quad (2)$$

where m_s is the mass concentrations of organic matter (OC × 1.6), ρ_s is the organic density (1.35 g/cm^3), and k_{org} is the organic hygroscopicity parameter (0.06) (Liu et al., 2017).

2.4 pH uncertainty

Two extreme scenarios were evaluated to estimate the pH uncertainty based on the measurement uncertainties of input data (Murphy et al., 2017). Sensitivity tests of pH to input data (see Section 3.3) suggest that simulated pH increase with the cation concentrations (i.e., TNH_x, TNa, K^+, Ca^{2+}, and Mg^{2+}) increasing as well as the anion concentrations (i.e., TH_2SO_4, TNO_3, and TCl), T and RH decreasing. Moreover, the pH value has a positive correlation with OC concentrations via Eqs. (1 and 2). Therefore, cation and OC concentrations were adjusted up to within their maximum positive uncertainties, and anions, RH and T were adjusted down within their maximum negative uncertainties, which represented the pH_{max} case; for pH_{min} case, cations and OC concentrations were adjusted down, and anions, RH and T were adjusted up. Figure 1 suggests that pH_{max} cases lead to 6 % (slope − 1) errors for all sites, and pH_{min} cases can result in approximately 10 % deviations. Thus, pH uncertainties were set to be −9–6 %, −13–6 %, −12–6 %, −11–6 %, and −10–5 % for U-ZZ, U-AY, R-AY, R-XX, and R-PY sites, respectively.

2.5 Model validation

The reliability of pH estimation using the ISORROPIA-II thermodynamic model depends on several assumptions, such as the equilibrated gas and particle phases (Pye et al., 2019). Thus, the predicted and observed semi-volatile species (e.g., $NH_{3(g)}/NH_{4(aq)}^+$, $HCl_{(g)}/Cl_{(aq)}^-$, and $HNO_{3(g)}/NO_{3(aq)}^-$) are compared in Fig. S2. Observed and predicted NH_4^+, Cl^-, and NO_3^- exhibit significant correlations, have correlation coefficients (r) above 0.95 and slopes near 1 at the five sites. In addition, NH_3 concentrations are in good agreement ($r > 0.95$) with slopes between 0.89 (U-ZZ) and 1.13 (R-PY). These results suggest the excellent performance of ISORROPIA-II for modeling these species. The

differences in the slopes of NH_4^+ (Fig. S2b) and NH_3 (Fig. S2e) between U-ZZ and R-PY sites were probably attributed to the unbalanced charge of input WSIIs (see Text S1 for more details of calculation) with average equivalent ratios (Fig. S3) of 0.99 ± 0.13 (U-ZZ) and 1.20 ± 0.12 (R-PY). However, Song et al. (2018) argued that ion balance was not a key factor for pH calculation in the forward mode, because the forward mode calculations account for additional constraints imposed by the partitioning of semi-volatile species. To verify this, we adjusted the measured NH_4^+ concentration, which was most sensitive to pH modeling (see Section 3.3), to fit the ion balance, and reran the pH calculation. As shown in Fig. S4, re-predicted NH_4^+ and NH_3 concentrations have better performance (r = 0.99, 0.94 < slopes < 1.06) with input concentrations at two sites than before. However, re-calculated pH values change slightly, and these deviations are included in the range of pH uncertainty discussed in Section 2.4. Therefore, the little differences in NH_x partitioning between the model and measurement among the five sites were acceptable for pH calculation.

Correlations between the predicted and measured HNO_3 and HCl are weak. Similar problems were found in the northeast U.S. and Beijing. These discrepancies were potentially due to measurement uncertainties brought about by low gas concentrations, the interference of coarse-mode particles, non-volatile cation measurement artifacts, uncertainties in the thermodynamic constants, and kinetic limitations to mass transfer (Ding et al., 2019, Haskins et al., 2018; Pye et al., 2019; Liu et al., 2017). Pye et al. (2019) suggested that ISORROPIA-II yields a mean activity coefficient of (H^+, Cl^-) that may result in the higher predicted HCl concentration. HNO_3 can be partition to both fine and coarse modes, thereby affecting predicted fine-mode nitrate concentrations (Nah et al., 2018). The best semi-volatile species for evaluation of pH modeling depend on the fraction of the gas phase. In this work, most of

208 HNO_3 and HCl concentrated in the particle phase, and thus they are not suited to test the model (Guo
209 et al., 2016).

210 The $PM_{2.5}$ pH was also calculated by the E-AIM (Version IV) model to evaluate the performance
211 of ISORROPIA-II using the observed data (RH > 60 %) of the U-ZZ site as an example. Close
212 correlation (r = 0.89) is found between two models with a slope of 0.95 (Fig. S5). The pH values in
213 ISORROPIA-II are 0.46 ± 0.15 units higher than those in E-AIM. These values are comparable to the
214 founding by Liu et al. (2017) and Song et al. (2018), which is possibly due to the differences of activity
215 coefficient values between the ISORROPIA-II and E-AIM models (Pye et al., 2019). Overall, the
216 predicted pH values using ISORROPIA-II are effective in this work.

217 **3 Results and discussion**

218 **3.1 Haze episodes**

219 During the sampling periods, five monitoring sites simultaneously experienced a long-lasting and
220 large-scale haze episode. Time series of the concentrations of major species (i.e., NH_3, NH_4^+, SO_4^{2-},
221 and NO_3^-) and meteorological parameters at the U-ZZ site as an example are presented in Fig. 2, and
222 other sites are integrated into Fig S6 with the mean values listed in Table 3. Three study cases were
223 classified on the basis of similar meteorological conditions and WSIIs levels at the five sites. The
224 WSIIs concentration, T, and RH gradually increased in the southern wind during Case 1 (January
225 12−14). Case 3 (January 21–25) was characterized by decreased WSII concentrations, T, and RH with
226 the northeastern wind. Even though the total WSIIs (TWSIIs) concentrations were comparable, the
227 chemical components of WSIIs were various between Cases 1 and 3 (Table 3). In particular, NO_3^-,
228 NH_4^+, and NH_3 concentrations in Case 1 were higher than those in Case 3 at all sites. Conversely,

229 SO_4^{2-} concentrations in Case 1 were lower than those in Case 3. Wang et al. (2018a) reported that the
230 southern cities of Henan Province (e.g., Nanyang, Shangqiu, Zhoukou, and Zhumadian) had relatively
231 higher ammonia emissions than the cities involved in this study. Moreover, the northeastern air masses
232 from the Jing–Jin–Ji regions were easily enriched with sulfate (Wang et al., 2019b; Wang et al., 2018c).
233 Evidently, back trajectory frequency analysis (see Text S2 for more details of the discussion) confirmed
234 that sampling sites during Cases 1 and 3 (Figs. S7a and c) were predominantly influenced by the
235 southern and northeastern air masses, respectively.

236 Elevated WSIIs concentrations during Case 2 (January 14–21) were under high T and RH
237 conditions with variable wind directions. In this case, local emissions played a key role in WSIIs (Fig.
238 S7b) with average NH_4^+, SO_4^{2-}, and NO_3^- concentrations that ranged from 31.9 ± 12.5 μg/m^3 (U-ZZ)
239 to 47.6 ± 13.1 μg/m^3 (R-AY), 32.9 ± 12.5 μg/m^3 (R-XX) to 46.8 ± 16.9 μg/m^3 (R-AY), and 58.0 ± 18.3
240 μg/m^3 (U-AY) to 76.8 ± 21.1 μg/m^3 (R-AY), respectively. Note that higher concentrations of NH_4^+,
241 NH_3, and TNH_x during Case 2 were recorded at rural sites than those at urban sites. Moreover, NH_3
242 levels in this work were higher than those in other studies summarized in Table S1. Agricultural
243 emissions, including livestock waste, N-fertilizer application, and humans, were the top three ammonia
244 contributors in Henan Province (Wang et al., 2018a), which may result in elevated ammonia
245 concentrations at rural sites.

246 **3.2 pH of $PM_{2.5}$ at the urban and rural sites**

247 Figure 3 exhibits the predicted $PM_{2.5}$ pH values, H^+_{air}, and AWC at the five sites, pH uncertainties
248 based on the pH_{max} and pH_{min} calculations are presented in Fig. S8. $PM_{2.5}$ have consistent moderate
249 acidity during this haze episode, with median (min–max) pH values of 4.5 (3.8–5.2), 4.8 (3.9–5.8), 4.9

250 (4.1–6.2), 5.1 (4.7–6.3), and 5.2 (4.8–6.5,) at U-ZZ, U-AY, R-XX, R-AY, and R-PY, respectively. As
251 summarized in Table 1, $PM_{2.5}$ pH values were close to the results of other cities in China (e.g., Beijing,
252 Xi'an, and Tianjin), but higher than other countries (e.g., Singapore, USA, and Greece). Compared to
253 the rural sites in the USA, pH values were roughly 3 units higher at the R-AY, R-XX, and R-PY sites.
254 Moreover, statistical values of pH (Table S2) during three cases show higher pH values at rural sites
255 than those at urban sites, especially for the U-ZZ and R-PY sites during Case 1 despite their pH
256 uncertainties (Section 2.4).

257 The pH values (Table S2) of the five sites during Cases 2 and 3 were comparable but slightly
258 lower than those during Case 1. As shown in Fig. S9, predicted pH values present better correlations
259 with H^+_{air} concentrations rather than AWC. Particle hydronium ion aqueous concentration depends on
260 both the presence of ions and the amount of particle AWC (Guo et al., 2015). Moreover, H^+_{air} was
261 closely associated with the NH_3 mixing ratios, and higher NH_3 always corresponded to lower H^+_{air} (Liu
262 et al., 2017). High correlations ($r > 0.5$) between H^+_{air} and TWSIIs (Table S3) imply that local pH was
263 significantly affected by the TWSIIs levels, and probably resulting in the high acidity during Case 2.
264 H^+_{air} was also correlated with individual chemical species (e.g., TNH_x, TH_2SO_4, TNO_3, and TCl).
265 Therefore, the diversity of pH in Cases 1 and 3 may be partly owing to the different proportions of
266 particle- and gas-phase constituents that will be discussed in detail below. In addition, high correlations
267 between RH and H^+_{air} (Table S3) suggest the major role of meteorological conditions in particle pH.
268 Given the Case 2 was less affected by regional transport, the diurnal patterns of median pH values of
269 the five sites (Fig. 4) indicate that pH values during nighttime were 0.3 (R-PY)–0.5 (U-ZZ) units higher
270 than those during the daytime. Similar results were also found in other cities (e.g., Beijing, Tianjin,

271 southern Canada, and the USA) (Battaglia et al., 2017; Ding et al., 2019; Guo et al., 2015; Murphy et
272 al., 2017; Shi et al., 2019), resulting from the diurnal trends of T and RH (Fig. 4f). After sunrise, high
273 T facilitated the dissociation of particle-phase ammonium (e.g., NH_4NO_3) and led to a rapid loss of
274 AWC (Guo et al., 2015; Saraswati et al., 2019).

275 **3.3 Sensitivity tests of pH**

276 To explore the dominant factors that determine the local particle pH level and resulting in the high
277 pH at rural sites, sensitivity tests of pH to chemical species (i.e., TNH_x, TH_2SO_4, TNO_3, TCl, TNa, K^+,
278 Ca^{2+}, and Mg^{2+}) and meteorological parameters (i.e., T and RH) were performed. Firstly, the real-time
279 measured values of a variable (e.g., TNH_x) and average values of other parameters (i.e., TH_2SO_4, TNO_3,
280 TCl, TNa, K^+, Ca^{2+}, Mg^{2+}, T and RH) during Case 2 were input into ISORROPIA-II to investigate the
281 sensitivity of local pH to this variable (i.e., TNH_x) (Ding et al., 2019), and results are listed in Table 4
282 and Fig. S10. In addition, a given range for a variable for all sites with corresponding average values
283 of other parameters was simulated to compare its effects on pH among five sites (Figs. 5 and S11). The
284 chosen variation range for each variable was close to the observed minimum and maximum values
285 (Table S4), which aims to better reflect the actual observation conditions. The degree of sensitivity
286 was represented as the relative standard deviation (%RSD) of the re-calculated pH values. RSD
287 calculates the absolute value of the coefficient of variation, which helps us to determine how small or
288 large is the standard deviation when compared to the mean of the re-calculated pH data set. Therefore,
289 when the re-calculated pH data set has a higher RSD value, this variable can change the pH easier and
290 is more important for local pH.

291 As shown in Table 4, the most important factor that influenced particle pH during Case 2 was

292 TNH_x, followed by TH_2SO_4 at the five sites, and the U-ZZ site was also affected by TNO_3. The acidity
293 of $PM_{2.5}$ is governed by the phase partitioning of semi-volatile gases such as NH_3, HNO_3, and HCl
294 (Pye et al., 2019). $(NH_4)_2SO_4$, NH_4HSO_4, and NH_4NO_3, which are mainly formed through
295 neutralization reactions between NH_3 with SO_4^{2-} and HNO_3 orderly according to the regime of local
296 ammonia, are the most abundant components of $PM_{2.5}$ in winter haze in this region (Wang et al., 2019c;
297 Pathak et al., 2008). Therefore, particle pH was driven by TNH_x, TH_2SO_4, and TNO_3. TNa, TCl, and
298 crustal ions (i.e., K^+, Ca^{2+}, and Mg^{2+}) have less influence on the predicted pH values, because these
299 species were at low concentrations, together accounting for lower than 10 % of TWSIIs. However,
300 since the low volatility of these cations allows them to preferentially neutralize sulfates over NH_3, the
301 role of crustal dust and sea spray in particle pH cannot be ignored when the mass fraction of these ions
302 are high in typical pollution events (e.g., sandstorm) or areas (e.g., coastland) (Allen et al., 2015; Guo
303 et al., 2018; Vasilakos et al., 2018). In addition to chemical species, T was more sensitive to local pH
304 than RH at the five sites, which is similar to the finding in Beijing and Canada (Ding et al., 2019; Tao
305 and Murphy, 2019). This result can be explained by the remarkable influence of T on the solubility and
306 dissociation constants of the partitioning of $NH_{3(g)}/NH_{4(aq)}^+$ (Hennigan et al., 2015).

307 Figures 5 and S11 compare the sensitive degrees of pH to input data among different sites. Except
308 for TNH_x, the sensitivities of pH to TH_2SO_4, TNO_3, and other ions at urban sites were more significant
309 than those at rural sites, particularly at U-ZZ sites of 7.2 % and 14.8 % of RSD to TH_2SO_4 and TNO_3,
310 respectively. To gain insight into the differences of pH sensitivity among the five sites, sensitivity tests
311 of pH to TH_2SO_4, TNO_3, and TNH_x were calculated using the fixed TNO_3 (67.5 μg/m^3) and TH_2SO_4
312 (36.5 μg/m^3) concentrations under the average meteorological conditions of five sites (i.e., T = 2.5 ℃

313 and RH = 60 %). These chosen values were close to the average values of the five sites during Case 2
314 (i.e., 36.4 ± 15.4 μg/m^3 for SO_4^{2-}, 67.5 ± 23.5 μg/m^3 for TNO_3, 2.5 ± 1.5 ℃ for T, and 59.3 ±14.0 %
315 for RH), and other chemical species were set to be zero. As shown in Fig. 6, sensitivities of pH to
316 TH_2SO_4 and TNO_3 increase with the decrease in TNH_x concentration, particularly when the TNH_x
317 concentrations are lower than 60 μg/m^3 and 40 μg/m^3, respectively. Therefore, the pH changes tended
318 to become more sensitive to TH_2SO_4 and TNO_3 at the U-ZZ site (Fig. 5e, f) with the lowest TNH_x
319 concentrations (46.8 ± 14.7 μg/m^3). All these results may be explained by the presence of excess
320 ammonia that will be discussed below.

321 Sensitivity tests suggest (Fig. 5, S10, and S11) that particle pH gradually grows with increased
322 cation and decreased anion concentrations. Specifically, the TNH_x concentration that increased from
323 25 μg/m^3 to 90 μg/m^3 can promote particle pH by 3.5 (U-ZZ)–4.5 (R-AY) units. The crustal cations
324 and sea spray have limited effects on pH, but a 10-fold increase in these species still can increase
325 predicted pH values by about 0.1 units. TH_2SO_4, and TNO_3 that increased from 10 μg/m^3 to 80 μg/m^3,
326 and 1 μg/m^3 to 125 μg/m^3 can reduce the pH values by 1.5 (R-PY)–4.0 (U-ZZ), and 0.2 (R-AY)–1.4
327 (U-ZZ) units, respectively. In addition, a 20 ℃ (–5 ℃ to 15 ℃) and 65 % (30 % to 95 %) increase
328 drops the pH by approximately 1.3 and 2.7 units at the five sites, respectively. Corresponding to the
329 observed data during Case 2 (Table 3), lower TNH_x concentrations and higher T values were probably
330 responsible for the higher acidity at urban sites than those at rural sites. Moreover, Figure 6 shows that
331 particle pH increase with decreasing TH_2SO_4 (Fig. 6a) or increasing TNO_3 (Fig. 6b), particularly when
332 the TNH_x is at high concentration. These results indicate that predicted pH will be enhanced by
333 increasing the TNO_3/TH_2SO_4 ratio, which is consistent with the observation in Beijing (Xie et al.,

2019). All these may be due to the elevated ammonia partitioning with nitrate fraction increase, and nitrate-rich particles would absorb more water compared to the sulfate-rich particles (Xie et al., 2019). Based on the above, higher TNH_x (Table 3) and TNO_3/TH_2SO_4 ratios (2.9 ± 0.6 and 1.7 ± 0.6 for Cases 1 and 3 respectively) during Case 1 may lead to the higher pH values than those during Case 3, even though the TWSIIs levels were comparable. In the long run, the decreasing sulfate concentration in $PM_{2.5}$ accompanied with increasing nitrate concentration has been recorded during haze episodes in China, because strong actions were taken to reduce the coal consumption in recent years (Tian et al., 2017; Wang et al., 2017). Considering the ammonia in the atmosphere of North China might still be increasing (Liu et al., 2018), future acidity of $PM_{2.5}$ during winter haze episodes is expected to become increasingly less acidic in this area. A more careful analysis is needed to test this inference, however, because fine-mode particle remains a relatively constant pH of 0–2 despite a 70 % reduction in sulfates in the USA (Vasilakos et al., 2018; Weber et al., 2016).

3.4 Role of ammonia on pH

It has been suggested that unusually high levels of NH_3 can increase pH, on average, a 5-fold to 10-fold increase in the NH_3 levels leads to a one-unit change in pH (Nah et al., 2018; Weber et al., 2016; Guo et al., 2017). To examine the effects of major indicators of ammonia (i.e., TNH_x, Required-NH_x, and Excess-NH_x, see Text S3 for more details of calculation) on aerosol acidity, particle pH was calculated by using a wide range of TNH_x (25–130 $\mu g/m^3$) and average values of other parameters during Case 2 (Table 3) of each site. Simultaneously, the concentrations of TNH_x, Required-NH_x, Excess-NH_x, and corresponding pH values are illustrated in Fig. 7. An "*S*-curve" growth trend of pH to increasing TNH_x appears with the inflection point around the Required-NH_x concentration. In the

355 case when the input TNH_x concentration is lower than the Required-NH_x, the growth rate of pH
356 increase with TNH_x increasing, otherwise, the pH growth flattens out, which is similar to the findings
357 of Weber et al. (2016) and Bougiatioti et al. (2016). In the process of increasing NH_3 concentration,
358 NH_3 reacted with SO_4^{2-} and HNO_3 orderly, during when large amounts of H^+ were consumed and pH
359 values rapidly increased. Theoretically, the Required-NH_x plus nonvolatile cations can neutralize all
360 anions regardless of the phase partitioning and bisulfate formation, and thus changes in TNH_x around
361 the Required-NH_x concentrations have a significant impact on particle pH. Subsequently, dissolving
362 Excess-NH_x into the particles became difficult, and pH values increased slowly (Ding et al., 2019;
363 Seinfeld and Pandis, 2016). Therefore, the underlying reason why TNH_x concentrations lower than 60
364 $\mu g/m^3$ and 40 $\mu g/m^3$ elevated the pH sensitivities (Fig. 6) to TH_2SO_4 and TNO_3 is that the Excess-NH_x
365 will be exhausted under the case of TH_2SO_4 and TNO_3 that ranged from 10 $\mu g/m^3$ to 100 $\mu g/m^3$,
366 respectively. On the other hand, the pH values of the five sites at the Required-NH_x concentrations are
367 near 3.0, which is in coincidence with the pH value of Beijing in the no-excess-NH_x cases (Liu et al.,
368 2017). Therefore, the presence of Excess-NH_x in the aerosol was likely important for the less acidic of
369 $PM_{2.5}$ and can enhance the pH values by 1.5 (U-ZZ)–2 (R-PY) units. Considering that the Excess-NH_x
370 concentrations at rural sites (e.g., 30.1 ± 6.2 $\mu g/m^3$ at R-PY) were higher than those at urban sites (e.g.,
371 14.8 ± 4.1 $\mu g/m^3$ at U-ZZ), and thus Excess-NH_x concentrations may drive the pH values of rural sites
372 higher than those of urban sites.

373 **3.5 Implications of regional transport**

374 From the above discussion, the differences of pH among three cases indicate that the underlying
375 influence of regional transport on local particle pH cannot be neglected by differing the chemical

components of $PM_{2.5}$ and meteorological conditions. In particular, the median pH values (Table S2) of Case 1, during when the air masses transported from the south of sampling regions, increased by 0.2–0.9 units than those during Cases 2 and 3. Aqueous formations of sulfate are strongly dependent on particle pH. Chen et al. (2016) reported that the aqueous-phase sulfate production rates from NO_2 and O_3 oxidation of SO_2 had a positive correlation with particle pH during the Beijing haze events. When pH exceeded approximately 4.5 (higher than this value at rural sites in this work), NO_2-oxidation dominated the sulfate formation, and its reaction rate increased by one order of magnitude with the rise of pH by one unit. Thus, air masses transported from rural and agricultural regions may promote the sulfate formation in urban aerosols. In addition to sulfate, higher aerosol pH favors partitioning of TNO_3 toward aerosol NO_3 rather than gaseous HNO_3 and thus elevating the particle mass concentration (Nenes et al., 2019; Weber et al., 2016). Sampling regions in this study are located in the transport route for Beijing (MEP, 2017), thereby frequently affecting its local particle pH. The lifetimes of NH_3 (1–5 days or less) and NH_4^+ (1–15 days) in the atmosphere are sufficient for transporting to Beijing during a haze episode (Aneja, 2000; Lefer et al., 1999; Warneck, 1988). Ding et al. (2019) have also observed that $PM_{2.5}$ pH from the southwest direction was generally higher than that from the northern direction in Beijing. Therefore, the particle pH in Beijing may be enhanced when southern air masses from this region accompany elevated-pH particles and high ammonia levels.

4 Conclusions

An experiment was performed using a series of high-time-resolution instruments in two urban (i.e., U-ZZ and U-AY) and three rural sites (i.e., R-AY, R-XX, and R-PY) in Henan Province during a large-scale and long-lasting haze episode. The ISORROPIA-II model was used to investigate the pH

value and its driving factors. $PM_{2.5}$ exhibited moderate acidity with median pH values of 4.5 (3.8–5.2), 4.8 (3.9–5.8), 4.9 (4.1–6.2), 5.1 (4.7–6.3), and 5.2 (4.8–6.5,) at U-ZZ, U-AY, R-XX, R-AY, and R-PY, respectively. The pH values at rural sites were slightly higher than those at urban sites.

The predicted pH values of $PM_{2.5}$ were significantly affected by the WSIIs levels, different proportions of particle- and gas-phase constituents, and meteorological parameters. Sensitivity tests show that TNH_x, followed by TH_2SO_4, were the important factors that influenced the predicted pH at the five sites. In addition, T was more sensitive to local pH than RH. Generally, particle pH rose with the increase in cation and the decrease in the anion, T, and RH. Further study suggests that predicted pH will be enhanced by increasing the TNO_3/TH_2SO_4 ratio. Therefore, elevated TNH_x concentrations and lower T were probably responsible for the higher pH values at rural sites than those at urban sites, and higher TNH_x and TNO_3/TH_2SO_4 ratios during Case 1 may lead to the higher pH values than those during Case 3.

An "*S*-curve" growth trend of pH to increasing TNH_x was found with the inflection point around the Required-NH_x concentration. Moreover, the pH values of the five sites at the Required-NH_x concentrations are near 3.0, and the presence of Excess-NH_x in the aerosol can enhance the pH values by 1.5 (U-ZZ)–2 (R-PY) units, and thus Excess-NH_x was likely important for the less acidic of $PM_{2.5}$ during the severe haze episodes in this region. Considering that the Excess-NH_x concentrations at rural sites were higher than those at urban sites, Excess-NH_x concentrations may drive the pH values of rural sites higher than those of urban sites.

The underlying influence of regional transport on local particle pH cannot be neglected by differing the chemical components of $PM_{2.5}$ and meteorological conditions. Air masses transported

418 from rural and agricultural regions with elevated pH particles and high ammonia levels may promote
419 the secondary particle formation in urban aerosols. Therefore, ammonia should be involved in the
420 regional strategy for improving the air quality in China.
421
422 *Data availability. All data in this work are available by contacting the corresponding author Shasha*
423 *Yin (shashayin@zzu.edu.cn)*
424
425 *Author contributions. Shasha Yin and Ruiqin Zhang designed and led this study. Shasha Yin was*
426 *responsible for all observations and data collection. Lingling Wang, Yuqing Li, Chen Wang, and Weisi*
427 *Wang interpreted the data and discussed the results. Shenbo Wang wrote the paper.*
428
429 *Competing interests. The authors declare that they have no conflict of interest.*
430 **Acknowledgment**
431 This work was supported by the National Key R&D Program of China (No. 2017YFC0212403)
432 and the National Natural Science Foundation of China (No. 41907187). We thank Qi Hao and Liuming
433 Yang for their contributions to the field observations.
434 **References**
435 Allen, H. M., Draper, D. C., Ayres, B. R., Ault, A., Bondy, A., Takahama, S., Modini, R. L., Baumann,
436 K., Edgerton, E., Knote, C., Laskin, A., Wang, B., and Fry, J. L.: Influence of crustal dust and sea
437 spray supermicron particle concentrations and acidity on inorganic NO_3^- aerosol during the 2013
438 Southern Oxidant and Aerosol Study. Atmos. Chem. Phy., 15, 10669−10685, 2015.

Aneja, V. P., Chauhan, J. P., Walker, J. T.: Characterization of atmospheric ammonia emissions from swine waste storage and treatment lagoons. J. Geophy. Res.-Atmos., 105, 11535−11545, 2000.

Battaglia, M. A., Douglas, S., and Hennigan, C. J.: Effect of the urban heat island on aerosol pH, Environ. Sci. Technol., 51, 13095−13103, 2017.

Behera, S. N., Betha, R., Liu, P., Balasubramanian, R.: A study of diurnal variations of $PM_{2.5}$ acidity and related chemical species using a new thermodynamic equilibrium model. Sci. Total Environ., 452, 286−295, 2013.

Boucher, O., Anderson, T. L.: General circulation model assessment of the sensitivity of direct climate forcing by anthropogenic sulfate aerosols to aerosol size and chemistry. J. Geophy. Res.-Atmos., 100, 26117−26134, 1995.

Bougiatioti, A., Nikolaou, P., Stavroulas, I., Kouvarakis, G., Weber, R., Nenes, A., Kanakidou, M., Mihalopoulos, N.: Particle water and pH in the eastern Mediterranean: source variability and implications for nutrient availability. Atmos. Chem. Phy., 16, 4579−4591, 2016.

Bureau of Statistics of Henan (NBH), 2018. Henan Statistical Yearbook. China Statistics Press, Beijing. Accessed date: Dec. 2019.

Cheng, Y., Zheng, G., Wei, C., Mu, Q., Zheng, B., Wang, Z., Gao, M., Zhang, Q., He, K., Carmichael, G.: Reactive nitrogen chemistry in aerosol water as a source of sulfate during haze events in China. Sci. Adv., 2, e1601530−e1601530, 2016.

Clegg, S. L., Brimblecombe, P., Wexler, A. S.: The thermodynamic model of the system H^+−NH_4^+−SO_4^{2-}−NO_3^-−H_2O at tropospheric temperatures. J. Phy. Chem. A, 102, 2137−2154, 1998.

460 Ding, J., Zhao, P., Su, J., Dong, Q., Du, X., Zhang, Y.: Aerosol pH and its driving factors in Beijing.
461 Atmos. Chem. Phy., 19, 7939−7954, 2019.
462 Dockery, D. W., Cunningham, J., Damokosh, A. L., Neas, L. M., Spengler, J. D., Koutrakis, P., Ware,
463 J. H., Raizenne, M., Speizer, F. E.: Health effects of acid aerosols on North American children:
464 respiratory symptoms. Environ. Health Persp., 104, 500−505, 1996.
465 Guo, H., Sullivan, A. P., Campuzanojost, P., Schroder, J. C., Lopezhilfiker, F. D., Dibb, J. E., Jimenez,
466 J. L., Thornton, J. A., Brown, S. S., Nenes, A.: Fine particle pH and the partitioning of nitric acid
467 during winter in the northeastern United States. J. Geophy. Res.-Atmos., 121, 10−355, 2016.
468 Guo, H., Weber, R. J., Nenes, A.: High levels of ammonia do not raise fine particle pH sufficiently to
469 yield nitrogen oxide-dominated sulfate production. Sci. Rep., 7, 12109, 2017.
470 Guo, H., Xu, L., Bougiatioti, A., Cerully, K. M., Capps, S. L., Hite, J. R., Carlton, A. G., Lee, S., Bergin,
471 M. H., Ng, N. L.: Fine-particle water and pH in the southeastern United States. Atmos. Chem.
472 Phy., 15, 5211−5228, 2015.
473 Guo, H., Nenes, A., and Weber, R. J.: The underappreciated role of nonvolatile cations on aerosol
474 ammonium-sulfate molar ratios, Atmos. Chem. Phys., 18, 17307–17323, 2018.
475 Haskins, J. D., Jaegle, L., Shah, V., Lee, B. H., Lopez-Hilfiker, F. D., Campuzano-Jost, P., Schroder, J.
476 C., Day, D. A., Guo, H. Y., Sullivan, A. P., Weber, R., Dibb, J., Campos, T., Jimenez, J. L., Brown,
477 S. S., and Thornton, J. A.: Wintertime gas-particle partitioning and speciation of inorganic
478 chlorine in the lower troposphere over the northeast United States and coastal ocean, J. Geophys.
479 Res.-Atmos., 123, 12897−12916, 2018
480 Healy, R. M., Sciare, J., Poulain, L., Crippa, M., Wiedensohler, A., Prévôt, A. S. H., Baltensperger, U.,

Sarda-Estève, R., McGuire, M. L., Jeong, C.-H., McGillicuddy, E., O'Connor, I. P., Sodeau, J. R., Evans, G. J., and Wenger, J. C.: Quantitative determination of carbonaceous particle mixing state in Paris using single-particle mass spectrometer and aerosol mass spectrometer measurements, Atmos. Chem. Phys., 13, 9479–9496, 2013.

Hennigan, C. J., Izumi, J., Sullivan, A. P., Weber, R. J., and Nenes, A.: A critical evaluation of proxy methods used to estimate the acidity of atmospheric particles, Atmos. Chem. Phys., 15, 2775–2790, 2015.

Hu, G., Zhang, Y., Sun, J., Zhang, L., Shen, X., Lin, W., Yang, Y.: Variability, formation and acidity of water-soluble ions in $PM_{2.5}$ in Beijing based on the semi-continuous observations. Atmos. Res., 145, 1−11, 2014.

Huang, X., Song, Y., Li, M., Li, J., Huo, Q., Cai, X., Zhu, T., Hu, M., Zhang, H.: A high-resolution ammonia emission inventory in China. Global Biogeochem. Cy., 26, GB1030, 2012.

Larssen, T., Lydersen, E., Tang, D., He, Y., Gao, J., Liu, H., Duan, L., Seip, H .M., Vogt, R. D., Mulder, J.: Acid rain in China. Environ. Sci. Technol., 40, 418−425, 2006.

Lefer, B. L., Talbot, R. W., Munger, J. W.: Nitric acid and ammonia at a rural northeastern US site. J. Geophy. Res.-Atmos., 104, 1645−1661, 1999.

Li, Y. J., Sun, Y., Zhang, Q., Li, X., Li, M., Zhou, Z., Chan, C. K.: Real-time chemical characterization of atmospheric particulate matter in China: A review. Atmos. Environ., 158, 270−304, 2006.

Liu, J., Bergin, M., Guo, H., King, L., Kotra, N., Edgerton, E., Weber, R. J.: Size-resolved measurements of brown carbon in water and methanol extracts and estimates of their contribution to ambient fine-particle light absorption. Atmos. Chem. Phy., 13, 12389−12404, 2013.

Liu, M., Song, Y., Zhou, T., Xu, Z., Yan, C., Zheng, M., Wu, Z., Hu, M., Wu, Y., Zhu, T.: Fine particle pH during severe haze episodes in northern China. Geophys. Res. Lett., 44, 5213−5221, 2017.

Liu, W., Lin, S., and Hu, G.: Characterizing remarkable changes of severe haze events and chemical compositions in multi-size airborne particles (PM_1, $PM_{2.5}$ and PM_{10}) from January 2013 to 2016−2017 winter in Beijing, China, Atmos. Environ., 189, 133−144, 2018.

Markovic, M. Z., Vandenboer, T. C., Murphy, J. G.: Characterization and optimization of an online system for the simultaneous measurement of atmospheric water-soluble constituents in the gas and particle phases. J Environ. Monitor., 14, 1872−1884, 2012.

Meng, Z., Lin, W., Jiang, X., Yan, P., Wang, Y., Zhang, Y. M., Jia, X. F., Yu, X. L.: Characteristics of atmospheric ammonia over Beijing, China. Atmos. Chem. Phy., 11, 6139−6151, 2011.

Meng, Z., Xu, X., Lin, W., Ge, B., Xie, Y., Song, B., Jia, S., Zhang, R., Peng, W., Wang, Y.: Role of ambient ammonia in particulate ammonium formation at a rural site in the North China Plain. Atmos. Chem. Phy., 18, 167−184, 2017.

MEP: 2017 air pollution prevention and management plan for the Beijing-Tianjin-Hebei region and its surrounding areas, http://dqhj.mee.gov.cn/dtxx/201703/t20170323_408663.shtml (last access: 18 August 2019), 2017.

Meskhidze, N., Chameides, W. L., Nenes, A., Chen, G.: Iron mobilization in mineral dust: Can anthropogenic SO_2 emissions affect ocean productivity? Geophys. Res. Lett., 30, 2003.

Murphy, J. G., Gregoire, P. K., Tevlin, A. G., Wentworth, G. R., Ellis, R. A., Markovic, M. Z., VandenBoer, T. C.: Observational constraints on particle acidity using measurements and modelling of particles and gases, Faraday Discuss., 200, 379−395, 2017.

Nah, T., Guo, H., Sullivan, A. P., Chen, Y., Tanner, D. J., Nenes, A., Russell, A., Ng, L. N., Huey, L. G., Weber, R. J.: Characterization of aerosol composition, aerosol acidity, and organic acid partitioning at an agriculturally intensive rural southeastern US site. Atmos. Chem. Phy. 18, 11471−11491. 2018.

National Bureau of Statistics (NBS), 2016. China Statistical Yearbook. China Statistics Press, Beijing. Accessed date: Sept. 2019.

Nenes, A., Pandis, S. N., Pilinis, C.: ISORROPIA: A new thermodynamic equilibrium model for multiphase multicomponent inorganic aerosols. Aquat. Geochem., 4, 123−152, 1998.

Nenes, A., Pandis, S. N., Weber, R. J., and Russell, A.: Aerosol pH and liquid water content determine when particulate matter is sensitive to ammonia and nitrate availability, Atmos. Chem. Phys. Discuss., in review, 2019.

Ostro, B., Lipsett, M., Wiener, M.B., Selner, J.C.: Asthmatic responses to airborne acid aerosols. Am. J. Public Health, 81, 694−702, 1991.

Panteliadis, P., Hafkenscheid, T., Cary, B., Diapouli, E., Fischer, A., Favez, O., Quincey, P., Viana, M., Hitzenberger, R., Vecchi, R.: ECOC comparison exercise with identical thermal protocols after temperature offset correction: instrument diagnostics by in-depth evaluation of operational parameters. Atmos. Meas. Tech., 8, 779−792, 2014.

Pathak, R. K., Louie, P. K., Chan, C. K.: Characteristics of aerosol acidity in Hong Kong. Atmos. Environ., 38, 2965−2974, 2004.

Pathak, R.K., Wu, W.S., Wang, T.: Summertime $PM_{2.5}$ ionic species in four major cities of China: nitrate formation in an ammonia-deficient atmosphere. Atmos. Chem. Phys. 9, 1711–1722, 2008.

544 Pye, H. O. T., Nenes, A., Alexander, B., Ault, A. P., Barth, M. C., Clegg, S. L., Collett Jr., J. L., Fahey,
545 K. M., Hennigan, C. J., Herrmann, H., Kanakidou, M., Kelly, J. T., Ku, I.-T., McNeill, V. F.,
546 Riemer, N., Schaefer, T., Shi, G., Tilgner, A., Walker, J. T., Wang, T., Weber, R., Xing, J., Zaveri,
547 R. A., and Zuend, A.: The acidity of atmospheric particles and clouds, Atmos. Chem. Phys.
548 Discuss., in review, 2019.
549 Rumsey, I. C., Cowen, K. A., Walker, J. T., Kelly, T. J., Hanft, E. A., Mishoe, K., Rogers, C., Proost,
550 R., Beachley, G. M., Lear, G.: An assessment of the performance of the Monitor for AeRosols
551 and GAses in ambient air (MARGA): a semi-continuous method for soluble compounds. Atmos.
552 Chem. Phy., 14, 5639−5658, 2014.
553 Saraswati, Sharma, S. K., Saxena, M., Mandal, T. K.: Characteristics of gaseous and particulate
554 ammonia and their role in the formation of secondary inorganic particulate matter at Delhi, India.
555 Atmos. Res., 218, 34−49, 2019.
556 Seinfeld, J. H. and Pandis, S. N.: Atmospheric Chemistry and Physics: From Air Pollution to Climate
557 Change, 2nd Edition, John Wiley and Sons, Inc., Hoboken, New Jersey, USA, 2006.
558 Seinfeld, J. H. and Pandis, S. N.: Atmospheric Chemistry and Physics: From Air Pollution to Climate
559 Change (3rd edition), John Wiley and Sons, Inc., Hoboken, New Jersey, USA, 2016.
560 Shen, J., Liu, X., Ying, Z., Fangmeier, A., Goulding, K., Zhang, F.: Atmospheric ammonia and
561 particulate ammonium from agricultural sources in the North China Plain. Atmos. Environ., 45,
562 5033−5041, 2011.
563 Shi, G., Xu, J., Peng, X., Xiao, Z., Chen, K., Tian, Y., Guan, X., Feng, Y., Yu, H., Nenes, A.: pH of
564 aerosols in a polluted atmosphere: source contributions to highly acidic aerosol. Environ. Sci.

565 Technol., 51, 4289−4296, 2017.
566 Shi, X., Nenes, A., Xiao, Z., Song, S., Yu, H., Shi, G., Zhao, Q., Chen, K., Feng, Y., Russell, A. G.:
567 High-resolution data sets unravel the effects of sources and meteorological conditions on nitrate
568 and its gas-particle partitioning. Environ. Sci. Technol., 53, 3048−3057, 2019.
569 Shi, Z., Bonneville, S., Krom, M. D., Carslaw, K. S., Jickells, T. D., Baker, A. R., Benning, L. G.: Iron
570 dissolution kinetics of mineral dust at low pH during simulated atmospheric processing. Atmos.
571 Chem. Phy., 11, 995−1007, 2010.
572 Song, S., Gao, M., Xu, W., Shao, J., Shi, G., Wang, S., Wang, Y., Sun, Y., Mcelroy, M. B.: Fine particle
573 pH for Beijing winter haze as inferred from different thermodynamic equilibrium models. Atmos.
574 Chem. Phy., 18, 7423−7438, 2018.
575 Spurny, K. R.: Atmospheric acidic aerosols (review). J Aerosol Sci., 21, 1990.
576 Surratt, J. D., Chan, A. W. H., Eddingsaas, N. C., Chan, M. N., Loza, C. L., Kwan, A. J., Hersey, S.,
577 Flagan, R. C., Wennberg, P. O., Seinfeld, J. H.: Reactive intermediates revealed in secondary
578 organic aerosol formation from isoprene. P. Natl. Acad. Sci. USA., 107, 6640−6645, 2010.
579 Tao, Y. and Murphy, J. G.: The sensitivity of $PM_{2.5}$ acidity to meteorological parameters and chemical
580 composition changes: 10-year records from six Canadian monitoring sites. Atmos. Chem. Phy..
581 19, 9309−9320, 2019.
582 Tian, M., Wang, H., Chen, Y., Zhang, L., Shi, G., Liu, Y., Yu, J., Zhai, C., Wang, J., Yang, F.: Highly
583 time-resolved characterization of water-soluble inorganic ions in $PM_{2.5}$ in a humid and acidic
584 mega city in Sichuan Basin, China. Sci. Total Environ., 580, 224−234, 2017.
585 Vasilakos, P., Russell, A., Weber, R., and Nenes, A.: Understanding nitrate formation in a world with

586 less sulfate, Atmos. Chem. Phys., 18, 12765–12775, 2018.
587 Wang, C., Yin, S., Bai, L., Zhang, X., Gu, X., Zhang, H., Lu, Q., Zhang, R.: High-resolution ammonia
588 emission inventories with comprehensive analysis and evaluation in Henan, China, 2006–2016.
589 Atmos. Environ., 193, 11−23, 2018a.
590 Wang, G., Zhang, F., Peng, J., Duan, L., Ji, Y., Marreroortiz, W., Wang, J., Li, J., Wu, C., Cao, C.:
591 Particle acidity and sulfate production during severe haze events in China cannot be reliably
592 inferred by assuming a mixture of inorganic salts. Atmos. Chem. Phy., 18, 1−23, 2018b.
593 Wang, G., Zhang, R., Gomez, M. E., Yang, L., Levy, Z. M., Hu, M., Lin, Y., Peng, J., Guo, S., Meng,
594 J.: Persistent sulfate formation from London Fog to Chinese haze. P. Natl. Acad. Sci. USA., 113,
595 13630−13635, 2016.
596 Wang, H., Ding, J., Xu, J., Wen, J., Han, J., Wang, K., Shi, G., Feng, Y., Ivey, C., Wang, Y.: Aerosols
597 in an arid environment: The role of aerosol water content, particulate acidity, precursors, and
598 relative humidity on secondary inorganic aerosols. Sci. Total Environ., 646, 564−572, 2019a.
599 Wang, J., Zhao, B., Wang, S., Yang, F., Xing, J., Morawska, L., Ding, A., Kulmala, M., Kerminen, V.,
600 Kujansuu, J.: Particulate matter pollution over China and the effects of control policies. Sci. Total
601 Environ., 584, 426−447, 2017.
602 Wang, S., He, B., Yuan, M., Su, F., Yin, S., Yan, Q., Jiang, N., Zhang, R., Tang, X.: Characterization
603 of individual particles and meteorological conditions during the cold season in Zhengzhou using
604 a single particle aerosol mass spectrometer. Atmos. Res., 219, 13−23, 2019b.
605 Wang, S., Yan, Q., Yu, F., Wang, Q., Yang, L., Zhang, R., Yin, S., Wang, S., Yan, Q., Yu, F.: Distribution
606 and source of chemical elements in size-resolved particles in Zhengzhou, China: Effects of

607 regional transport. Aerosol Air Qual. Res., 18, 371−385, 2018c.
608 Wang, S., Yin, S., Zhang, R., Yang, L., Zhao, Q., Zhang, L., Yan, Q., Jiang, N., Tang, X.: Insight into
609 the formation of secondary inorganic aerosol based on high-time-resolution data during haze
610 episodes and snowfall periods in Zhengzhou, China. Sci. Total Environ., 660, 47−56, 2019c.
611 Warneck, P.: Chemistry of the Natural Atmosphere, Academic Press, San Diego, CA, 1988.
612 Watson, J. G.: Visibility: science and regulation. J Air Waste Manage., 52, 973−999, 2002.
613 Weber, R. J., Guo, H., Russell, A. G., and Nenes, A.: High aerosol acidity despite declining
614 atmospheric sulfate concentrations over the past 15 years, Nat. Geosci., 9, 282−285, 2016.
615 Wen, L., Chen, J., Yang, L., Wang, X., Xu, C., Sui, X., Yao, L., Zhu, Y., Zhang, J., Zhu, T.: Enhanced
616 formation of fine particulate nitrate at a rural site on the North China Plain in summer: The
617 important roles of ammonia and ozone. Atmos. Environ., 101, 294−302, 2015.
618 Xie, Y., Wang, G., Wang, X., Chen, J., Chen, Y., Tang, G., Wang, L., Ge, S., Xue, G., Wang, Y., and
619 Gao, J.: Observation of nitrate dominant $PM_{2.5}$ and particle pH elevation in urban Beijing during
620 the winter of 2017, Atmos. Chem. Phys. Discuss., in review, 2019.
621

Figure lists:

Fig. 1 pH uncertainties of the five sites based on two extreme scenarios of measurement uncertainty. Cations and organic carbon concentrations (OC) were adjusted up to within their maximum positive uncertainties, anions, relative humidity (RH) and temperature (T) were adjusted down within their maximum negative uncertainties, which represented the pH_{max} case; for pH_{min} case, cations and OC concentrations were adjusted down, and anions, RH and T were adjusted up. The color scale bar represents adjusted RH.

Fig. 2 Temporal variations of T, RH, wind speed (WS), wind direction (WD), and concentrations of NH_3, NH_4^+, SO_4^{2-}, and NO_3^- during three cases at the Zhengzhou (U-ZZ) site. The shaded areas represent the measurement uncertainties.

Fig. 3 Time series and box plot of predicted $PM_{2.5}$ pH, H^+_{air}, and aerosol water content (AWC) at the five sites. In each box, the top, middle and bottom lines represent the 75th, 50th, and 25th percentile of statistical data, respectively; the upper and lower whiskers represent the maximum and minimum values, respectively.

Fig. 4 (a)–(e) Diurnal patterns of median pH values, (f) average RH, and T of the five sites in Case 2. The upper and lower ends of the line represent the maximum and minimum values of pH, respectively. The color scale bar represents AWC concentration.

Fig. 5 Comparison of the sensitivities of $PM_{2.5}$ pH to T, RH, TCl ($HCl_{(g)} + Cl_{(aq)}^-$), TNH_x ($NH_{3(g)} + NH_{4(aq)}^+$), TNO_3 ($HNO_{3(g)} + NO_{3(aq)}^-$), and TH_2SO_4 (replaced by observed SO_4^{2-}) among the five sites. A given range for a variable for all sites with corresponding average values of other parameters was used as input to the ISORROPIA-II model. The range of the x-axis is close to the observed

643 minimum and maximum values in Case 2 (Table S4). The color scale bar represents the pH values.
644 The relative standard deviation (RSD) and range (Range) represent the sensitivity degree of pH to
645 this variable and range (min–max) of the re-predicted pH value in the test, respectively. The square
646 plots on the graph represent the average values of each variable observed in Case 2 with standard
647 deviation as an error bar.
648 Fig. 6 Particle pH calculated with fixed meteorological parameters (T = 275.5 K and RH = 60 %)
649 under different combinations of TNH_x and (a) TH_2SO_4 (Fixed TNO_3 = 67.5 μg/m^3) and (b) TNO_3
650 (Fixed TH_2SO_4 = 36.5 μg/m^3). The color scale bar represents the pH values. The markers on the
651 graph represent the average concentrations of TNH_x, TH_2SO_4, and TNO_3 at the five sites during Case
652 2 with standard deviation as error bar.
653 Fig. 7 Particle pH corresponds to increasing TNH_x at the five sites to examine the effects of major
654 indicators of NH_3 (i.e., TNH_x, Required-NH_x, and Excess-NH_x) on aerosol acidity. Particle pH was
655 calculated by using a wide range of TNH_x (25–130 μg/m^3) and average values of other parameters
656 during Case 2 of each site. The concentrations of TNH_x, Required-NH_x, and Excess-NH_x with
657 corresponding pH values are marked by a hollow box, hollow circle, and arrow respectively. The
658 yellow and blue background colors correspond to the NH_x-poor and NH_x-rich, respectively.
659

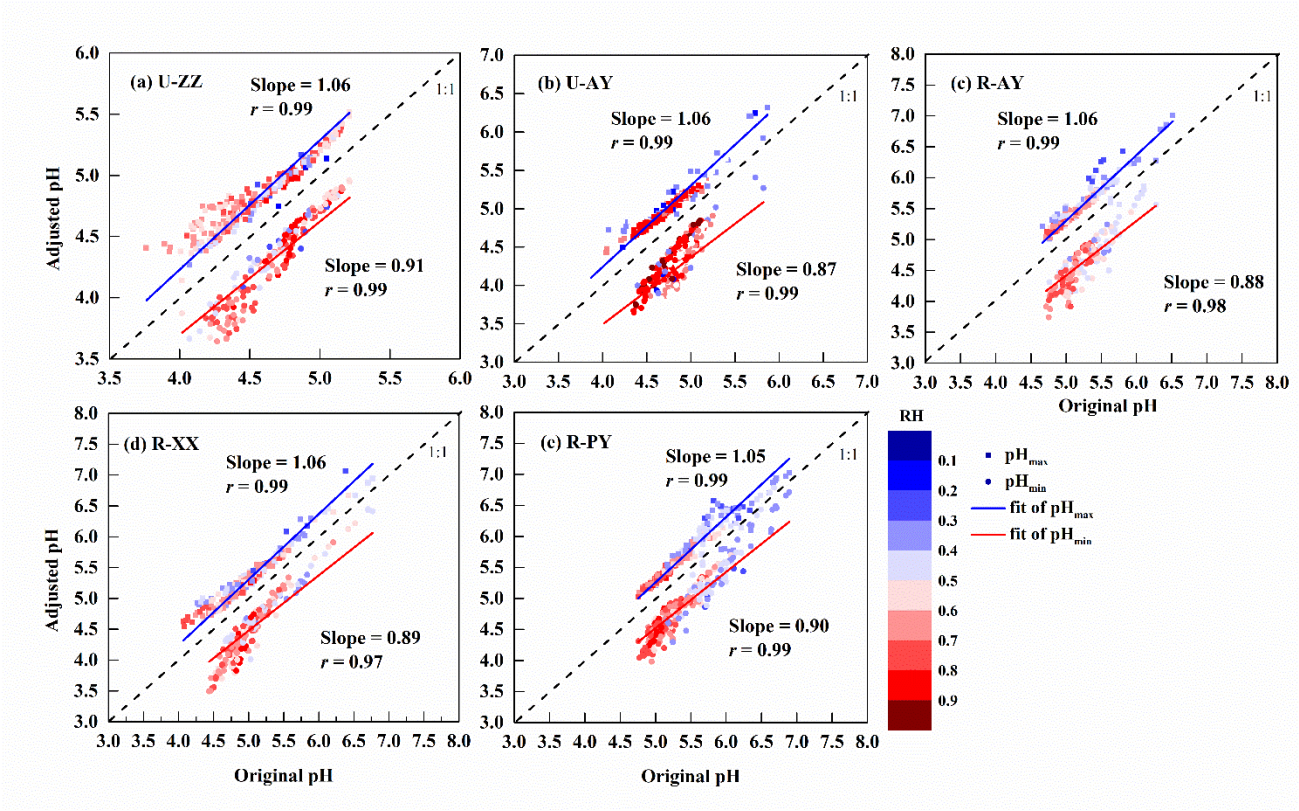

660

661 Fig. 1 pH uncertainties of the five sites based on two extreme scenarios of measurement uncertainty.

662 Cations and organic carbon concentrations (OC) were adjusted up to within their maximum positive

663 uncertainties, anions, relative humidity (RH) and temperature (T) were adjusted down within their

664 maximum negative uncertainties, which represented the pH_{max} case; for pH_{min} case, cations and OC

665 concentrations were adjusted down, and anions, RH and T were adjusted up. The color scale bar

666 represents adjusted RH.

667

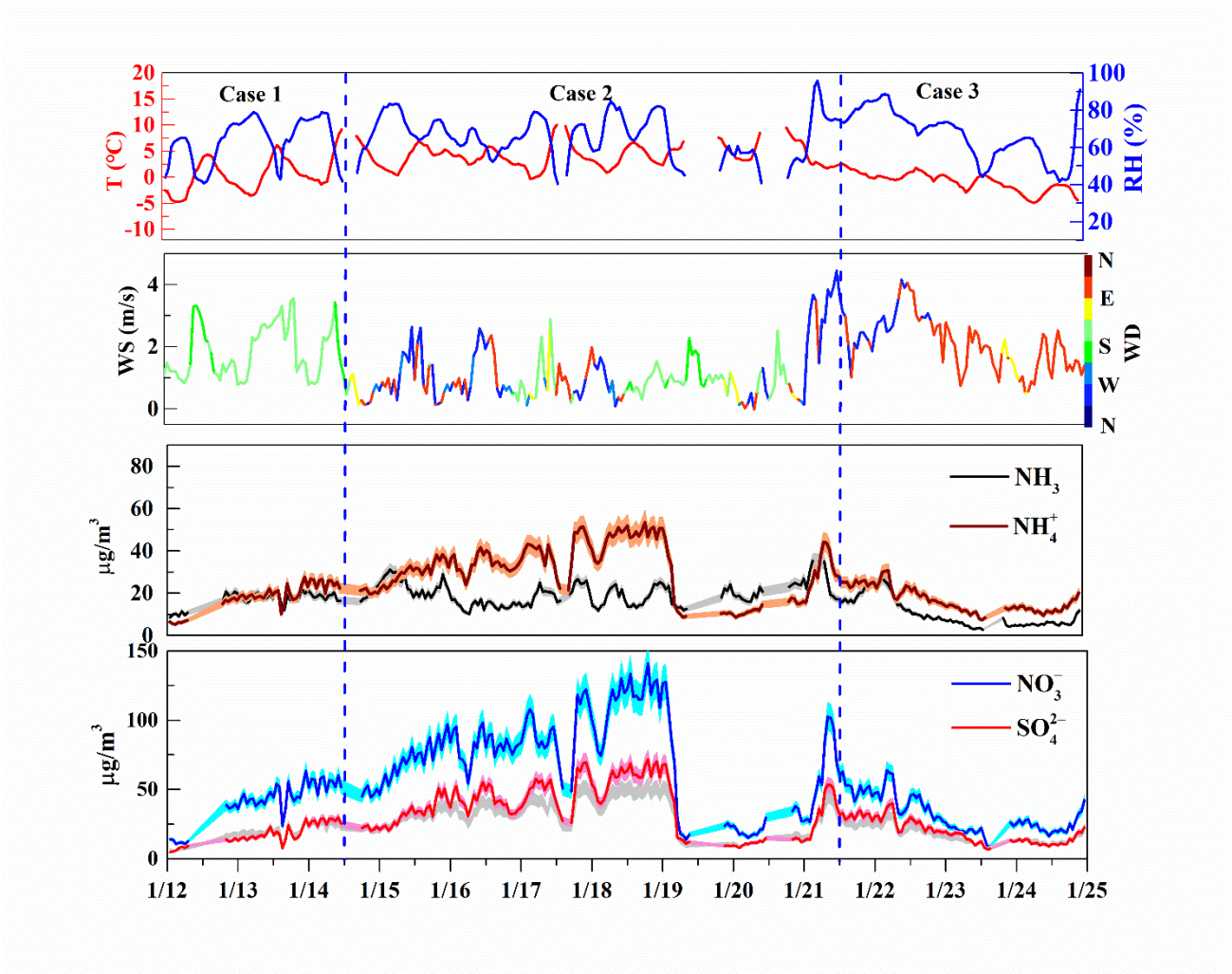

668

669 Fig. 2 Temporal variations of T, RH, wind speed (WS), wind direction (WD), and concentrations of

670 NH_3, NH_4^+, SO_4^{2-}, and NO_3^- during three cases at the Zhengzhou (U-ZZ) site. The shaded areas

671 represent the measurement uncertainties.

672

673

674

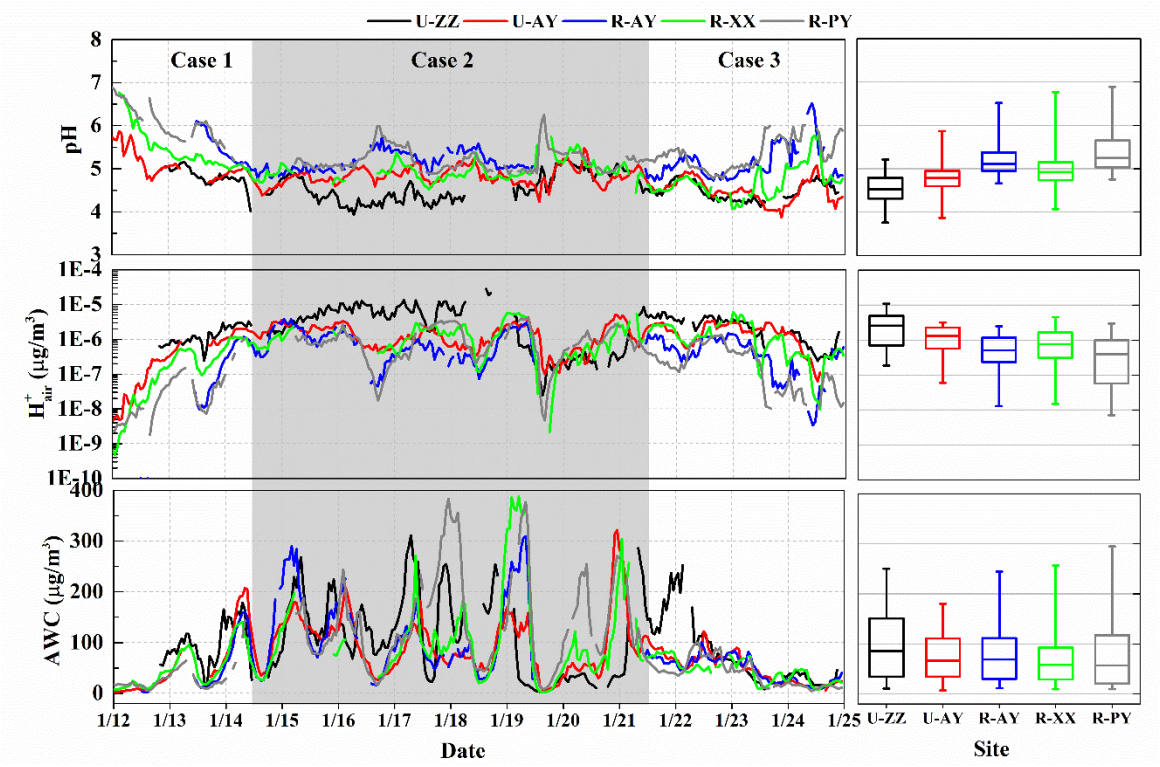

675

676 Fig. 3 Time series and box plot of predicted $PM_{2.5}$ pH, H^+_{air}, and aerosol water content (AWC) at the

677 five sites. In each box, the top, middle and bottom lines represent the 75th, 50th, and 25th percentile

678 of statistical data, respectively; the upper and lower whiskers represent the maximum and minimum

679 values, respectively.

680

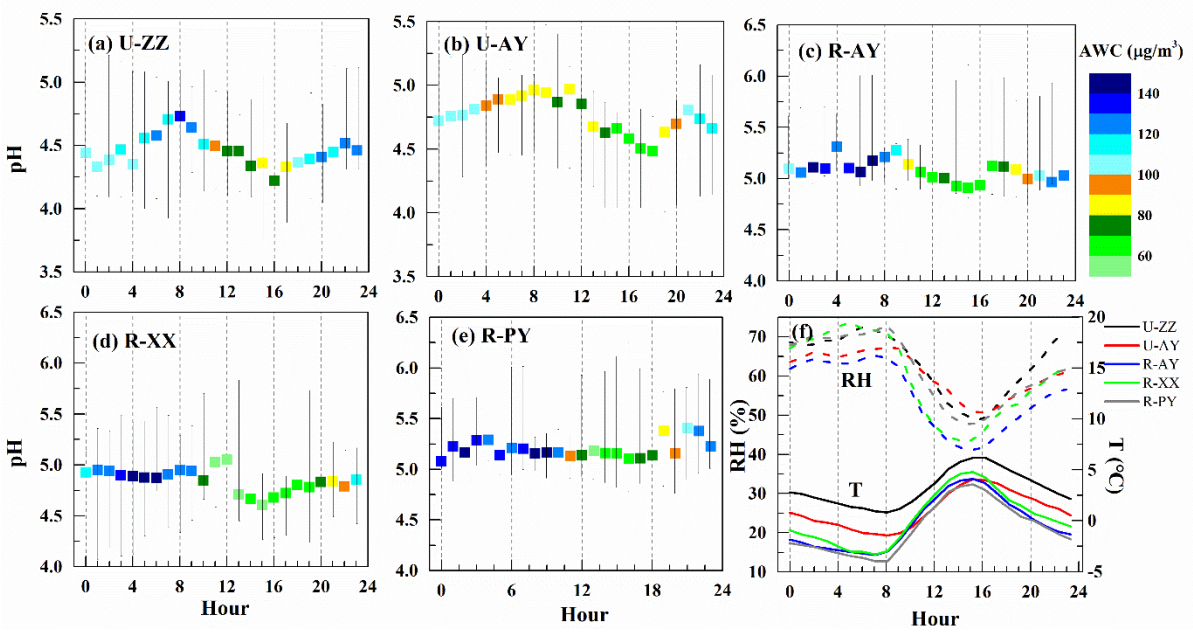

681

682 Fig. 4 (a)–(e) Diurnal patterns of median pH values, (f) average RH, and T of the five sites in Case 2.

683 The upper and lower ends of the line represent the maximum and minimum values of pH,

684 respectively. The color scale bar represents AWC concentration.

685

686

687

688

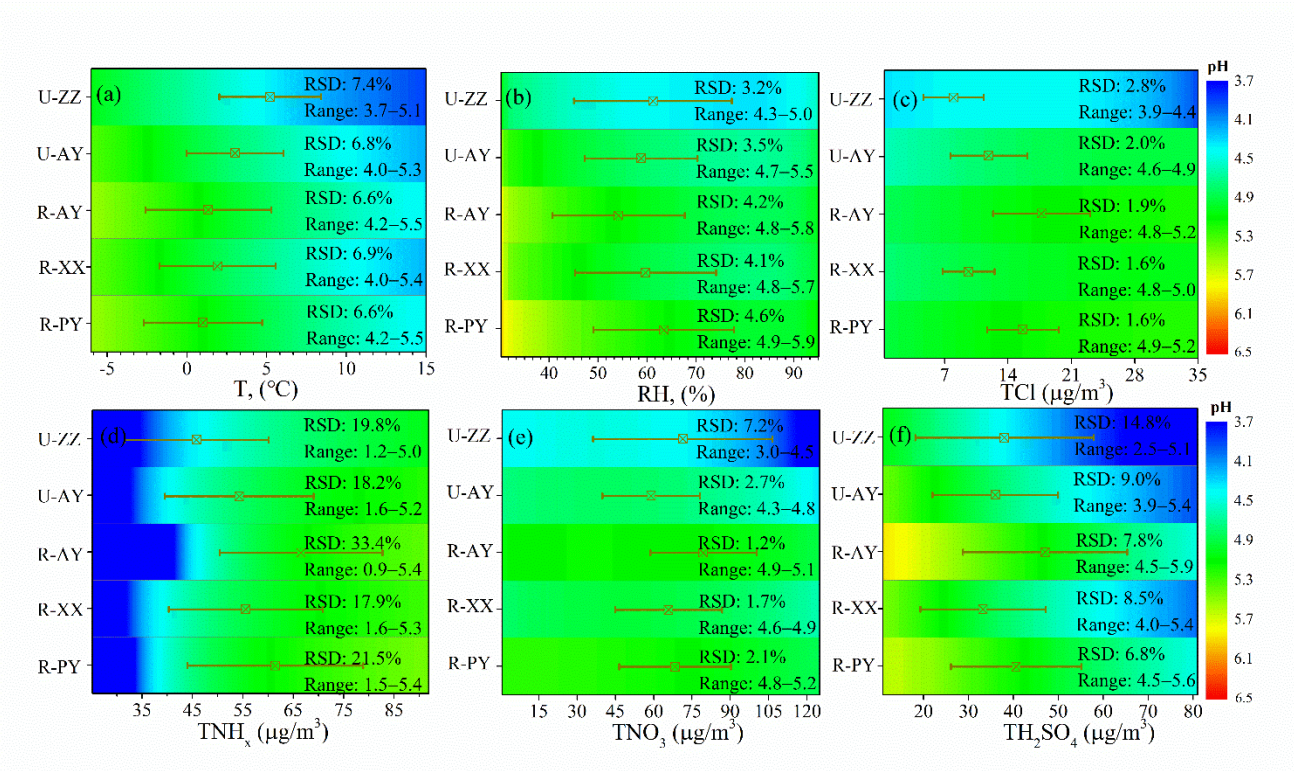

Fig. 5 Comparison of the sensitivities of $PM_{2.5}$ pH to T, RH, TCl ($HCl_{(g)} + Cl_{(aq)}^-$), TNH_x ($NH_{3(g)} + NH_{4(aq)}^+$), TNO_3 ($HNO_{3(g)} + NO_{3(aq)}^-$), and TH_2SO_4 (replaced by observed SO_4^{2-}) among the five sites. A given range for a variable for all sites with corresponding average values of other parameters was used as input to the ISORROPIA-II model. The range of the x-axis is close to the observed minimum and maximum values in Case 2 (Table S4). The color scale bar represents the pH values. The relative standard deviation (RSD) and range (Range) represent the sensitivity degree of pH to this variable and range (min–max) of the re-predicted pH value in the test, respectively. The square plots on the graph represent the average values of each variable observed in Case 2 with standard deviation as an error bar.

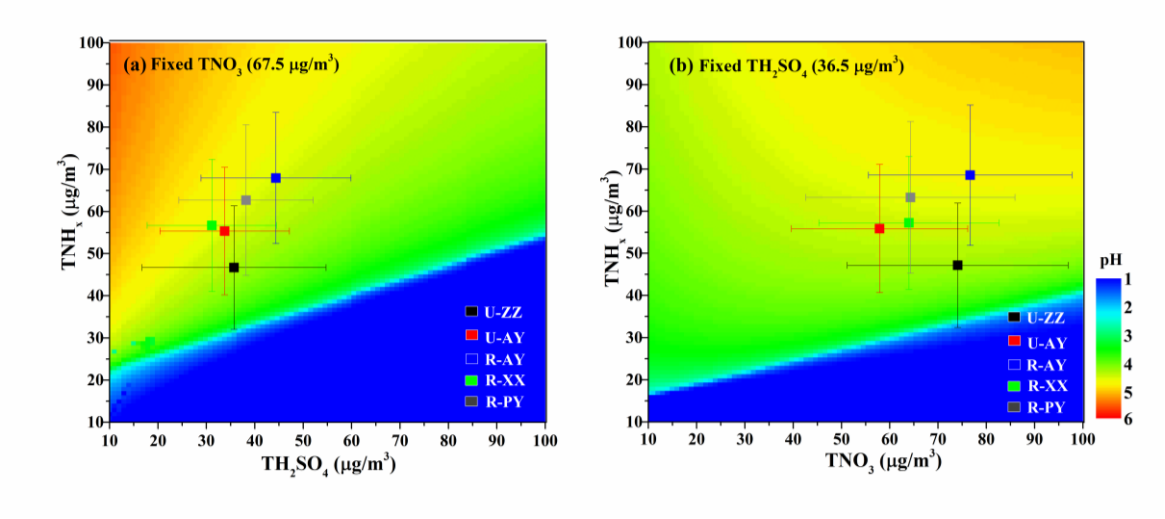

Fig. 6 Particle pH calculated with fixed meteorological parameters (T = 275.5 K and RH = 60 %) under different combinations of TNH_x and (a) TH_2SO_4 (Fixed TNO_3 = 67.5 μg/m^3) and (b) TNO_3 (Fixed TH_2SO_4 = 36.5 μg/m^3). The color scale bar represents the pH values. The markers on the graph represent the average concentrations of TNH_x, TH_2SO_4, and TNO_3 at the five sites during Case 2 with standard deviation as error bar.

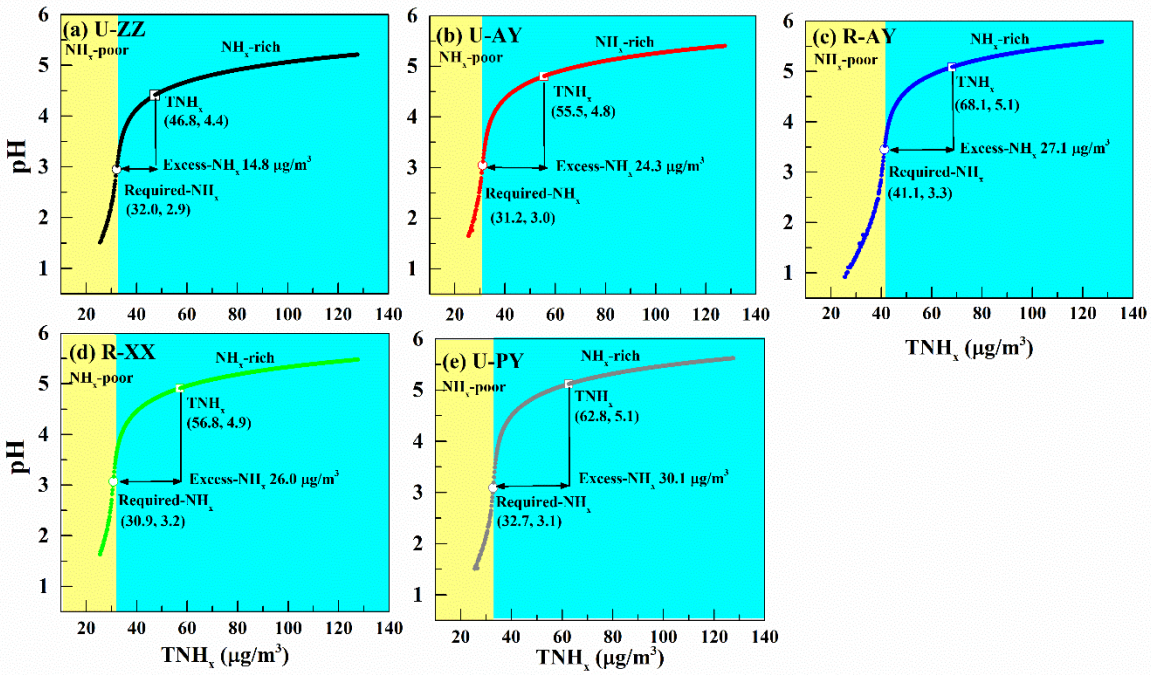

710

711 Fig. 7 Particle pH corresponds to increasing TNH_x at the five sites to examine the effects of major

712 indicators of NH_3 (i.e., TNH_x, Required-NH_x, and Excess-NH_x) on aerosol acidity. Particle pH was

713 calculated by using a wide range of TNH_x (25–130 $\mu g/m^3$) and average values of other parameters

714 during Case 2 of each site. The concentrations of TNH_x, Required-NH_x, and Excess-NH_x with

715 corresponding pH values are marked by a hollow box, hollow circle, and arrow respectively. The

716 yellow and blue background colors correspond to the NH_x-poor and NH_x-rich, respectively.

717

718

719 **Table lists:**

720 Table 1 Comparison of the particle pH values in this study (median, min–max) and other sites (mean ± standard deviation).

721 Table 2 Descriptions of the five sampling sites.

722 Table 3 Summary (mean ± standard deviation) of gaseous precursors (μg/m^3), water-soluble inorganic ions (μg/m^3), T (℃), and RH (%) during three cases

723 of haze periods at five monitoring sites.

724 Table 4 Sensitivity of pH to input data. The real-time measured values of a variable and the average values of other parameters during Case 2 were input

725 into the ISORROPIA II. The degree of sensitivity was represented as the relative standard deviation (%RSD) of the re-calculated pH values, higher RSD

726 implied higher sensitivity of this factor to pH and thus is more important for local pH.

727

728

729

730

731

732 Table 1 Comparison of the particle pH values in this study (median, min–max) and other sites (mean ± standard deviation).

	Observation site	Period	pH	Model	Reference
This study	Zhengzhou, China (Urban)	Jan 2018	4.5 (3.8–5.2)		
	Anyang, China (Urban)	Jan 2018	4.8 (3.9–5.8)		
	Anyang, China (Rural)	Jan 2018	4.9 (4.1–6.2)	ISORROPIA-II	
	Xinxiang, China (Rural)	Jan 2018	5.1 (4.7–6.3)		
	Puyang, China (Rural)	Jan 2018	5.2 (4.8–6.5)		
China	Beijing, China (Urban)	Feb 2017	4.5 ± 0.7	ISORROPIA-II	Ding et al., 2019
	Beijing, China (Urban)	Dec 2016	4.3 ± 0.4	ISORROPIA-II	Liu et al., 2017
	Beijing, China (Urban)	Jan–Feb 2015	4.5	ISORROPIA-II	Guo et al., 2017
	Xi'an, China (Urban)	Nove–Dec 2012	5.0	ISORROPIA-II	Guo et al., 2017
	Tianjin, China (Urban)	Dec–Jun 2015	4.9 ± 1.4	ISORROPIA-II	Shi et al., 2017
	Tianjin, China (Urban)	Aug 2015	3.4 ± 0.5	ISORROPIA-II	Shi et al., 2019
	Hohhot, China	Winter 2015	5.7	ISORROPIA-II	Wang et al., 2019
	PRD, China (Rural)	Fall-winter season 2012	0.81 ± 0.24	AIM-II model	Fu et al., 2015
	Hong Kong, China (Urban)	2001	0.25	AIM-II model	Pathak et al., 2004
Other countries	Singapore (Urban)	Sep–Nov 2011	0.60	AIM-IV model	Sailesh et al., 2013
	Northeastern US (Urban)	Feb–Mar 2015	0.07 ± 0.96	ISORROPIA-II	Guo et al., 2016
	Alabama, USA (Rural)	Jun–Jul 2013	1.94 ± 0.59	ISORROPIA-II	Guo et al., 2015
	Georgia, USA (Rural)	Aug–Oct 2016	2.2 ± 0.6	ISORROPIA-II	Nah et al., 2018
	Crete, Greece (Background)	Aug–Nov 2012	1.25 ± 1.14	ISORROPIA-II	Boucher et al., 2016

733

734 Table 2 Descriptions of the five sampling sites.

City	Classification	Site	Coordinate	Location	Surrounding environment	Emission (Gg) NH_3*	SO_2**	NO_x**
Zhengzhou	Urban	U-ZZ	34.82° N 113.54° E	West to the Zhengzhou downtown (Zhengzhou University)	Densely occupied residences, light industry, freeways and roads	39.2	36.7	31.8
Anyang	Urban	U-AY	36.09° N 114.41° E	East to the Anyang downtown (Anyang Environmental Protection Bureau)	Occupied residences, heavy industry and traffic roads	57.8	46.9	37.1
	Rural	R-AY	36.22° N 114.39° E	15 km north of Anyang city (Baizhuang town)	High ways, small villages, and cropland			
Xinxiang	Rural	R-XX	35.38° N 114.30° E	35 km northeast of Xinxiang city (Banzao town)	Small villages and cropland	72.1	8.9	19.6
Puyang	Rural	R-PY	36.15° N 115.10° E	44 km north of Puyang city (Liangcun town)	Small villages and cropland	39.6	3.4	3.2

735 * Data from a 2015-based NH_3 emission inventory (Wang et al., 2018a).

736 ** Data from Henan Statistical Yearbook of 2018 (BSH, 2018).

737

738

739

740

741 Table 3 Summary (mean ± standard deviation) of gaseous precursors (μg/m^3), water-soluble inorganic ions (μg/m^3), T (℃), and RH (%) during three cases

742 of haze periods at five sites.

	Case 1 (January 12−14)					Case 2 (January 14−21)					Case 3 (January 21−25)				
	U-ZZ	U-AY	R-AY	R-XX	R-PY	U-ZZ	U-AY	R-AY	R-XX	R-PY	U-ZZ	U-AY	R-AY	R-XX	R-PY
HNO_3	0.9 ± 0.2	0.7 ± 0.2	3.1 ± 0.2	3.0 ± 0.1	3.9 ± 0.1	1.3 ± 0.3	1.1 ± 0.3	3.7 ± 0.4	3.7 ± 0.5	4.2 ± 0.2	0.9 ± 0.3	0.7 ± 0.2	4.9 ± 1.0	3.3 ± 0.2	3.3 ± 0.2
NH_3	17.0 ± 3.7	19.6 ± 8.0	22.9 ± 6.3	21.6 ± 4.1	17.8 ± 3.7	19.5 ± 5.2	23.6 ± 6.5	25.2 ± 6.5	24.7 ± 9.9	26.5 ± 6.7	10.5 ± 6.9	8.8 ± 4.7	10.6 ± 4.7	8.4 ± 3.5	12.1 ± 3.5
HCl	0.1 ± 0.0	0.7 ± 0.6	0.5 ± 0.1	0.6 ± 0.1	1.8 ± 0.1	0.1 ± 0.1	0.4 ± 0.1	0.6 ± 0.2	0.6 ± 0.1	2.0 ± 0.1	0.1 ± 0.1	0.5 ± 0.1	1.7 ± 0.1	1.0 ± 0.4	1.5 ± 0.4
NO_3^-	41.5 ± 14.6	28.0 ± 14.6	43.0 ± 12.5	32.8 ± 12.9	25.2 ± 9.1	74.2 ± 32.9	58.0 ± 18.3	76.8 ± 21.1	64.1 ± 18.7	64.4 ± 21.7	32.4 ± 13.5	18.9 ± 5.4	26.0 ± 5.8	25.1 ± 6.7	18.8 ± 4.3
NH_4^+	18.6 ± 6.2	15.9 ± 8.3	21.8 ± 8.0	14.9 ± 6.2	12.8 ± 4.5	31.9 ± 12.5	35.2 ± 12.0	47.6 ± 13.1	35.6 ± 10.4	39.9 ± 14.9	17.4 ± 6.0	11.6 ± 4.4	14.3 ± 4.4	12.9 ± 4.0	10.1 ± 2.9
SO_4^{2-}	17.8 ± 7.2	14.4 ± 9.0	13.7 ± 10.0	10.0 ± 5.5	8.6 ± 2.3	38.3 ± 18.0	34.5 ± 13.0	46.8 ± 16.9	32.9 ± 12.5	39.2 ± 13.6	19.8 ± 8.6	15.1 ± 6.1	15.1 ± 7.3	14.4 ± 4.8	13.3 ± 4.0
Ca^{2+}	0.7 ± 0.5	0.5 ± 0.3	5.0 ± 2.2	0.8 ± 0.2	3.4 ± 0.3	0.5 ± 0.4	0.4 ± 0.4	2.2 ± 1.2	1.0 ± 0.3	3.3 ± 0.6	0.1 ± 0.1	0.2 ± 0.2	1.8 ± 0.7	0.5 ± 0.1	2.4 ± 0.5
Na^+	1.5 ± 0.2	1.0 ± 0.0	1.4 ± 0.4	0.7 ± 0.1	2.2 ± 0.1	1.6 ± 0.2	1.0 ± 0.1	1.4 ± 0.4	0.8 ± 0.1	2.2 ± 0.0	1.1 ± 0.2	1.0 ± 0.2	2.2 ± 0.4	1.3 ± 0.4	2.2 ± 0.2
Cl^-	7.5 ± 2.5	2.7 ± 3.4	6.6 ± 2.5	5.4 ± 1.5	6.3 ± 1.2	8.5 ± 3.2	12.0 ± 4.2	18.5 ± 5.0	9.7 ± 2.6	14.4 ± 3.8	3.3 ± 1.5	4.5 ± 1.6	6.9 ± 1.6	4.7 ± 0.9	5.4 ± 1.4
Mg^{2+}	0.2 ± 0.0	0.1 ± 0.0	0.4 ± 0.1	0.1 ± 0.0	0.5 ± 0.0	0.2 ± 0.0	0.1 ± 0.0	0.4 ± 0.4	0.1 ± 0.0	0.5 ± 0.1	0.2 ± 0.0	0.1 ± 0.0	0.4 ± 0.1	0.1 ± 0.1	0.4 ± 0.1
K^+	2.9 ± 0.7	1.4 ± 0.5	1.6 ± 0.6	1.6 ± 0.4	2.5 ± 0.6	4.4 ± 1.7	2.4 ± 0.7	2.9 ± 0.7	1.9 ± 0.6	3.7 ± 1.1	1.9 ± 0.7	0.9 ± 0.3	0.8 ± 0.3	0.8 ± 0.2	1.2 ± 0.4
T	0.3 ± 3.1	−0.9 ± 3.7	−1.8 ± 4.4	−2.0 ± 3.9	−1.7 ± 4.8	4.2 ± 2.2	2.6 ± 2.5	0.1 ± 2.8	1.2 ± 2.9	0.4 ± 3.0	−0.8 ± 1.8	−2.7 ± 1.8	−3.2 ± 1.9	−2.8 ± 2.6	−4 ± 2.3
RH	63.7 ± 12.1	60.3 ± 15.4	54.0 ± 16.0	58.5 ± 13.5	49.7 ± 14.5	66.0 ± 11.4	60.1 ± 9.9	58.6 ± 9.9	62.7 ± 11.6	65.8 ± 11.7	67 ± 13.1	63.7 ± 13.8	55.9 ± 13.6	59 ± 13.7	56.8 ± 16

743

744

Table 4 Sensitivity of pH to input data. The real-time measured values of a variable and the average values of other parameters during Case 2 were input into the ISORROPIA II. The degree of sensitivity was represented as the relative standard deviation (%RSD) of the re-calculated pH values, higher RSD implied higher sensitivity of this factor to pH and thus is more important for local pH.

	TH_2SO_4	TNH_x	TNO_3	TNa	TCl	Ca^{2+}	K^+	Mg^{2+}	RH	T
U-ZZ	12.1 %	12.8 %	6.1 %	0.1 %	0.3 %	3.3 %	0.3 %	0.2 %	1.3 %	2.7 %
U-AY	5.8 %	7.4 %	1.0 %	0.1 %	1.1 %	0.4 %	0.3 %	0.0 %	1.6 %	2.8 %
R-AY	6.5 %	10.9 %	1.4 %	0.1 %	0.7 %	1.2 %	0.2 %	0.3 %	1.9 %	2.7 %
R-XX	5.4 %	11.1 %	1.1 %	0.1 %	0.7 %	0.4 %	0.2 %	0.1 %	2.0 %	2.9 %
R-PY	4.7 %	9.4 %	1.5 %	0.0 %	0.7 %	0.5 %	0.4 %	0.1 %	2.3 %	3.1 %